Smart Mater. Struct. 21 (2012) 094010 (8pp) doi:10.1088/0964-1726/21/9/094010

A sharp interface model of compatible twin patterns in shape memory alloys

N T Tsou[1], J E Huber[1] and Y C Shu[2]

[1] Department of Engineering Science, University of Oxford, Parks Road, Oxford OX1 3PJ, UK
[2] Institute of Applied Mechanics, National Taiwan University, Taipei 106, Taiwan

E-mail: nien-ti.tsou@eng.ox.ac.uk

Received 10 March 2012, in final form 17 July 2012
Published 31 August 2012
Online at stacks.iop.org/SMS/21/094010

Abstract
The cubic–orthorhombic shape memory alloy system is studied using a sharp interface model based on the linear theory of compatible laminates. A computational method is developed to generate all possible compatible laminates for a given state of strain, and check whether these laminates satisfy exact compatibility conditions. The type of austenite–martensite interface that can form is dependent upon the detail of the martensite structure; the formation of flat and wedge-like austenite–martensite interfaces is explored. A full search is used to reveal the routes in strain space along which the two-phase structure can continuously evolve. A variety of laminate structures, some well known and some new, are reported. The methods developed are readily applied to other crystal systems, such as the tetragonal crystal system, in shape memory alloys or related materials.

(Some figures may appear in colour only in the online journal)

1. Introduction

Shape memory alloys are widely used as actuators and thin film devices. They are known to exhibit two significant properties, the shape memory effect and superelastic behaviour. The origin of these properties is the phase transformation from austenite to martensite. This results in different martensite variants being present, each variant having a distinct transformation strain. To accommodate these martensite variants and the austenite phase, shape memory alloy crystals usually adopt certain types of microstructure, such as fine twinned laminates, wedges, tunnel and tent structure [1, 2]. For the design of engineering components using shape memory alloys, an understanding of the role of microstructure is essential. In recent decades, the formation of microstructure in shape memory materials has been extensively studied. Ball and James [3] proposed a theory to explain fine phase mixtures based on energy minimization, and reveal the importance of compatibility between phases. Hane and Shield [4, 5] used related methods to study austenite–martensite twinned microstructures in the orthorhombic and monoclinic crystal systems. Bhattacharya and James [6] provide a geometrically nonlinear theory of martensite thin films and study untwinned austenite–martensite (A–M) interfaces. DeSimone and James [7] use linearized compatibility equations to develop a constrained theory for twinned laminate structures.

The formation of a compatible interface between the austenite and martensite phases is also rigorously discussed by Bhattacharya [1]. This is dependent upon the middle eigenvalue of the martensite transformation strain. If the middle eigenvalue is non-zero, then no exactly compatible A–M interface exists, and the resulting microstructures can be at best averagely compatible. However, common shape memory alloys typically have non-zero middle eigenvalue [1]. Thus, the compatible twin patterns that can form are limited. A typical austenite–martensite microstructure consists of a lamination of twinned martensite and a region of pure austenite phase, separated by a flat A–M interface [8, 9]. This arrangement is energetically favourable if the martensite part has an average strain state with zero middle eigenvalue. In general, this gives two unique orientations for the A–M interface. Another well known austenite–martensite microstructure is a wedge-like pattern. Structures of this type consist of two austenite–martensite laminates whose A–M interfaces intersect at a line in a midrib plane. The

 © 2012 IOP Publishing Ltd Printed in the UK & the USA

wedge-like arrangement can nucleate and grow from that line and this provides a mechanism through which the crystal can undergo the martensitic transformation [4, 5]. To understand microstructures in shape memory materials and their ability to evolve between austenite and martensite phases, it is of interest to study these austenite–martensite patterns and their microstructural rearrangement corresponding to different imposed strain states.

One of the main methods used to predict microstructures in shape memory materials is phase field modelling. The models typically use the time-dependent Ginzburg–Landau (TDGL) equations, with unit cell deformation as the order parameter [10, 11]. Alternatively, Shu and Yen [12, 13], Li *et al* [14, 15] and Lei *et al* [16] introduce the concept of hierarchical laminate structures and adopt the volume fractions of laminates as order parameters in their phase field model. However, since the phase field approach treats phase boundaries as diffuse interfaces, a fine mesh size is required in such models to discretize phase boundaries. Consequently, the method is computationally intensive, and two-dimensional problems or small regions of interest are usually considered. By contrast, sharp interface approaches treat a phase boundary as a discontinuity, across which the strain may jump. This gives a significant saving of computation and the study of large two-dimensional regions or complex microstructures becomes feasible. Roytburd *et al* [17] studied the martensitic transformation in several topologies of microstructure in constrained films. Goldsztein [18] introduced a tree diagram to represent laminated austenite and martensite phases and obtain the minimum energy microstructure. Although the sharp interface approach offers the potential to explore a wide range of microstructures, particular twin arrangements are commonly assumed. A motivation of the current work is to explore more broadly the set of possible twin structures that can form, and to use this approach to find routes in strain space along which the two-phase microstructure can continuously evolve.

A sharp interface compatibility model is developed and computational methods are used to search efficiently among the compatible laminates that can form in a cubic–orthorhombic shape memory alloy system. Similar to Goldsztein's work [18], a hierarchical binary tree diagram is used here to represent the microstructural arrangement. The present method does not find a single minimum energy state, but instead rapidly generates all possible compatible laminates corresponding to the given average strain state of a shape memory alloy crystal. The method relies on first generating compatible arrangements of pure martensite twins with the given average strain. The resulting martensite structures are then checked for exact or average compatibility. The ability of these martensite structures to form a compatible A–M interface is determined by examining their tree diagrams and strain states. In the present work, two forms of A–M interfaces are considered. The first is that of a single flat A–M phase boundary, with a compatible martensite laminate on one side. Secondly, we consider the formation of pairs of non-parallel A–M interfaces that meet along a line, giving a wedge-like microstructure. Microstructure maps are generated to show the routes in strain space along which the two-phase structure can continuously evolve. We show that the pure austenite state is linked to several well known configurations by continuous compatible paths.

2. Theory and methodology

2.1. Compatibility conditions

Consider a pair of phases (i, j) with stress-free transformation strain states $\boldsymbol{\epsilon}_i$, $\boldsymbol{\epsilon}_j$. For convenience of terminology, 'phase' will be used to refer to austenite, or any individual martensite variant. In the current work we adopt the framework of linear compatibility theory. A compatible interface with unit normal vector $\mathbf{n}$ then satisfies the well known compatibility equation [1, 7]:

$$\boldsymbol{\epsilon}_i - \boldsymbol{\epsilon}_j = \tfrac{1}{2}(\mathbf{a} \otimes \mathbf{n} + \mathbf{n} \otimes \mathbf{a}) \tag{1}$$

for some vector $\mathbf{a}$. A compatible interface can be formed whenever a unit vector $\mathbf{n}$ can be found that satisfies equation (1). In the present work, we limit our consideration to the case where the unit cell of each martensite phase has identical volume to that of the austenite phase, so that $\mathrm{tr}(\boldsymbol{\epsilon}_i) = 0$. This is convenient for comparison with the work of Lei *et al* [16]; however, the methods are readily extended to the more general case. Equation (1) can be solved by making use of the eigenvalues λ_k $(k = 1, \ldots, 3)$ and eigenvectors $\mathbf{e}_k$ of the 3×3 matrix $\mathbf{M} = \boldsymbol{\epsilon}_i - \boldsymbol{\epsilon}_j$. If solutions exist, and $\mathrm{tr}(\boldsymbol{\epsilon}_i) = 0$, then $\lambda_1 = -\lambda_3$ with $\lambda_2 = 0$. Two solutions of the interface normal $\mathbf{n}$ can then be obtained from [19]:

$$\mathbf{n} = \frac{\mathbf{e}_3 \pm \mathbf{e}_1}{\sqrt{2}}. \tag{2}$$

When more than two phases are present in the crystal, the microstructure may take the form of a periodic multi-rank laminate. In laminate structures, pairs of pure phases are layered together to form a rank-1 laminate, and similarly a pair of rank-1 laminates can be layered together to form a rank-2 structure. Here, a hierarchical binary tree diagram is used to represent the periodic structure of the laminate [18]. Figure 1 shows an example of a rank-2 tree diagram, which contains seven numbered nodes $i = 1, \ldots, 7$, each with a corresponding volume fraction f_i, and a corresponding state of average strain. Apart from nodes in the lowest level of the tree, each node is also associated with a vector $\mathbf{n}_i$ that gives the orientation of the compatible interface between the materials represented by its child nodes. The first node (root node) represents the entire microstructure while the nodes in the lowest level represent the pure phases. The volume fraction of each parent node is the sum of those in its child nodes, and the average strain at each node can be derived from

$$f_i = f_{2i} + f_{2i+1}, \qquad \boldsymbol{\epsilon}_i = f_{2i}\boldsymbol{\epsilon}_{2i} + f_{2i+1}\boldsymbol{\epsilon}_{2i+1}. \tag{3}$$

Suppose the volume fractions at the nodes, f_i, are unknown, but the crystal experiences a known macroscopic average strain $\boldsymbol{\epsilon}$. The volume fraction of the kth phase, $f_{(k)}$, can be estimated by making the approximation that the crystal

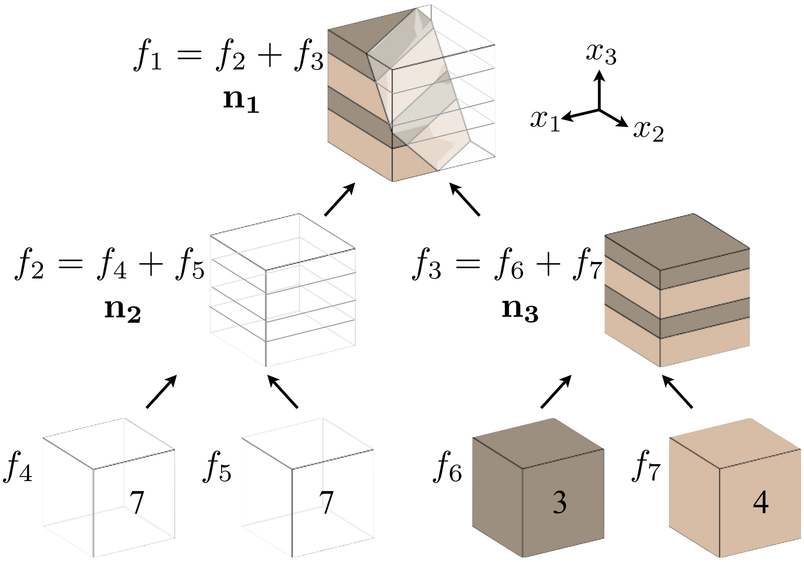

Figure 1. A rank-2 tree diagram showing volume fraction f_i of node i and interface normals of laminates.

is in a perfectly compatible state, free of stress. Then, the $f_{(k)}$ can be obtained by solving

$$\boldsymbol{\epsilon} = \sum_{k=1}^{N} f_{(k)}\boldsymbol{\epsilon}_{(k)} \tag{4}$$

$$1 = \sum_{k=1}^{N} f_{(k)}, \qquad 0 \le f_{(k)} \tag{5}$$

where N is the number of phases.

In the present work, we illustrate the method by focusing on the cubic–orthorhombic crystal system which has seven phases with strains $\boldsymbol{\epsilon}_{(i)}$ $(i = 1, \ldots, 7)$, given by

$$\begin{aligned}
\boldsymbol{\epsilon}_{(1,2)} &= \begin{bmatrix} \beta & 0 & 0 \\ 0 & \alpha & \pm\gamma \\ 0 & \pm\gamma & \alpha \end{bmatrix}, \qquad
\boldsymbol{\epsilon}_{(3,4)} = \begin{bmatrix} \alpha & 0 & \pm\gamma \\ 0 & \beta & 0 \\ \pm\gamma & 0 & \alpha \end{bmatrix}, \\
\boldsymbol{\epsilon}_{(5,6)} &= \begin{bmatrix} \alpha & \pm\gamma & 0 \\ \pm\gamma & \alpha & 0 \\ 0 & 0 & \beta \end{bmatrix}, \qquad
\boldsymbol{\epsilon}_{(7)} = \begin{bmatrix} 0 & 0 & 0 \\ 0 & 0 & 0 \\ 0 & 0 & 0 \end{bmatrix}.
\end{aligned} \tag{6}$$

Parameters α, β, and γ are material properties characterize the martensitic transformation strain. However, the restriction to $\mathrm{tr}(\boldsymbol{\epsilon}_{(i)}) = 0$ forces $\beta = -2\alpha$. Phases 1–6 are the orthorhombic martensite variants and phase 7 is the unstrained austenite. The symmetry of the system gives rise to six independent equations from equations (4) and (5) for seven unknown volume fractions, giving a general solution

$$\begin{aligned}
&[f_{(1)}\ f_{(2)}\ f_{(3)}\ f_{(4)}\ f_{(5)}\ f_{(6)}\ f_{(7)}]^{\mathrm{T}} \\
&\quad = \mathbf{f}_0 + t[-1\ -1\ -1\ -1\ -1\ -1\ 6]^{\mathrm{T}}.
\end{aligned} \tag{7}$$

Here $\mathbf{f}_0$ is a particular solution and parameter t is in the range of $0 \le t \le t_{\max}$ to ensure that $f_{(i)} \ge 0$. Thus, there is a continuous set of solutions for the phase volume fractions. It is always possible to set $f_{(7)} = 0$ in equation (7), so that a strategy for finding compatible microstructure arrangements is first to find a purely martensite structure with average strain $\boldsymbol{\epsilon}$, and then consider introducing a volume fraction of austenite as a separate step. In the first step, a unique solution for the martensite volume fractions exists.

The existence and uniqueness of solutions to equations (4) and (5) for the martensite volume fractions depend strongly on the number N of martensite phases, and their symmetry. For example, the tetragonal crystal system has $N = 3$ martensite crystal variants. Under the restriction of volume conservation, i.e. $\mathrm{tr}(\boldsymbol{\epsilon}_{(i)}) = 0$, equations (4) and (5) result in three linearly independent equations for the three unknown volume fractions, giving a unique solution. Similarly, the trigonal ($N = 4$) and orthorhombic ($N = 6$) crystal systems give either no solution or a unique solution for a given macroscopic strain state. However, in the monoclinic crystal system ($N = 12$), which is commonly adopted by nickel–titanium alloys [1], there are six linearly independent equations for 12 unknown volume fractions, resulting in non-unique solutions. Thus, the approach taken here, of solving equations (4) and (5) first, and then seeking compatible arrangements, works particularly well for tetragonal, trigonal and orthorhombic crystal systems. In crystal systems where a unique solution for the volume fractions cannot be obtained from equations (4) and (5), configurations can nevertheless be identified that simplify the laminate structure, for example by minimizing the number of variants present; see reference [19] for details. In the cubic–orthorhombic system, the martensite volume fractions corresponding to a given average strain in the martensite can be found uniquely.

With the martensite volume fractions known, we next distribute the total volume fraction for each phase, $f_{(k)}$, into the nodal volume fractions, f_i. DeSimone and James [7] provide a method for finding nodal volume fractions, which ensures that the microstructure satisfies compatibility equations averagely. However, for some special strain states, it is possible to find an exactly compatible structure. Structures of this type

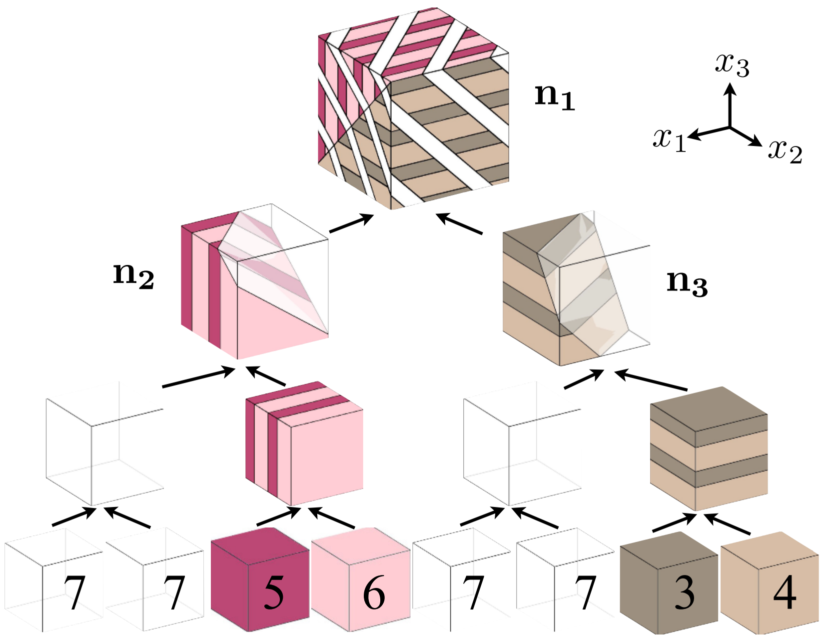

Figure 2. A tree diagram corresponding to a rank-3 wedge structure.

have one to one perfect alignment of phases, that satisfies the compatibility conditions exactly at every interface in the crystal.

Here we provide three conditions to check if a laminate pattern is an exactly compatible structure [19]. (i) Interfaces between distinct phases must have the same spacing wherever they meet at any higher level interface. In terms of the tree diagram, this means that the volume fraction ratios of corresponding sub-node pairs in each level should be identical, for example $f_4/f_5 = f_6/f_7$ in figure 1. (ii) The interface normals of any two nodes and the parent node that links them must be coplanar. For example, the interface normals of nodes 1, 2, 3 should satisfy $\mathbf{n}_1 \cdot (\mathbf{n}_2 \times \mathbf{n}_3) = 0$. A perfectly matched laminate pattern can be achieved if these two conditions are satisfied. However, a third condition is required to avoid local incompatibility. (iii) Wherever two phases meet, their interface must satisfy the compatibility requirement, equation (1). For example, in a rank-2 tree diagram, nodes 4 and 5 must be compatible across an interface with normal $\mathbf{n}_2$; similarly, nodes 4 and 6 must be compatible across an interface with normal $\mathbf{n}_1$. Note that the example structure shown in figure 1 satisfies conditions (i) and (ii), so the corresponding pattern is a perfect aligned laminate. However, the interface normal $\mathbf{n}_1$ cannot, in this example, satisfy compatibility for both node pairs 4, 6 and 5, 7 simultaneously. Thus, condition (iii) is violated, and the structure is not an exactly compatible laminate.

2.2. Conditions for flat and wedge-like A–M interfaces

In the present work, we focus on the most common case, that the middle eigenvalue of the martensitic transformation strain is non-zero. Thus, the formation of exactly compatible A–M interfaces is not possible, and only averagely compatible A–M interfaces can be found. A flat A–M interface is then possible provided that the imposed average strain state ϵ has a zero middle eigenvalue [20]. The A–M interface normal vector $\mathbf{n}_A$ can be obtained by solving equation (1) with the average strain of the martensite substituted for the left hand side of the equation. Figure 1 shows a typical rank-2 structure with a flat A–M interface. In general, the lowest level of the tree diagram for structures of this type has the austenite phases at exactly half of the nodes.

Next consider the formation of wedge-like A–M interfaces. A wedge structure can be built by joining two austenite-twinned martensite substructures, each with a flat A–M interface (see figure 2). The key requirement is that the flat A–M interfaces of both substructures must be non-parallel and meet at a line on the boundary between the substructures. If the two substructures have flat A–M interface normals $\mathbf{n}_2$ and $\mathbf{n}_3$, the projections of $\mathbf{n}_2$ and $\mathbf{n}_3$ into the boundary plane with normal $\mathbf{n}_1$ must match. This requirement is satisfied if $\mathbf{n}_1$, $\mathbf{n}_2$ and $\mathbf{n}_3$ are coplanar:

$$\mathbf{n}_1 \cdot (\mathbf{n}_2 \times \mathbf{n}_3) = 0 \tag{8}$$

where $\mathbf{n}_1 \nparallel \mathbf{n}_2 \nparallel \mathbf{n}_3$. The example shown in figure 2 is a rank-3 wedge structure consisting of one substructure identical to that of figure 1, and a second substructure with a similar arrangement of phases.

2.3. Search method for compatible laminate structures

The method described in sections 2.1 and 2.2 can be used to search for multi-rank compatible microstructures. To simplify the search, laminates of the minimum possible rank satisfying the imposed strain conditions will be found. Experimental observations indicate that structures of ranks 2 and 3 commonly occur in shape memory alloys, while higher rank structures are rarer [1]. The starting point is an average strain state ϵ imposed on a laminate of martensite variants only. Suppose that this imposed strain state requires m martensite variants to be present by equations (4) and (5). The minimum possible rank of laminate with m variants present is $\lceil \log_2 m \rceil$, where $\lceil x \rceil$ indicates the least integer greater than or equal to x. Meanwhile, the maximum rank that could be necessary for average compatibility is $(m-1)$, as guaranteed by the construction of DeSimone and James [7]. The minimum rank laminate may have rank $<(m-1)$ provided that $m \geq 4$. The distribution of the m martensite volume fractions among the $2^{\lceil \log_2 m \rceil}$ nodes in the lowest level of the tree diagram allows permutations. For example, with a rank-2 laminate, the tree diagram has four nodes in the lowest level. If only the three variants numbered 1–3 are present, it is necessary to divide the volume fraction of one variant between two nodes. This generates permutations such as '1123', '1223' and so forth, reading across the lowest level of the tree diagram. The existence of pairs of compatible solutions to equation (1) produces further structural permutations. An iteration procedure [21] is used to examine the set of permutations. We can also check the M–M interfaces for exact compatibility.

Next, the resulting martensite structures are tested for their ability to form flat or wedge-like A–M interfaces. If the imposed average strain $\boldsymbol{\epsilon}$ has a zero middle eigenvalue, a flat A–M interface can form and equation (1) gives the interface normal $\mathbf{n}_A$. To search for wedge-like A–M interfaces, we create a new tree diagram by inserting extra austenite nodes into the lowest level of the martensite tree diagram. This is conceptually the same as splitting the martensite laminate in half at the highest level interface and combining each half with austenite using new flat interfaces. If the new arrangement forms a compatible laminate, the requirement provided in equation (8) is checked. An example of this process can be seen in figure 2.

3. Application to austenite–martensite structures

In this section, the procedure of section 2 is applied to the study of austenite–martensite microstructures in the cubic–orthorhombic crystal system. We limit consideration to planar interfaces and illustrate the method using particular material parameters. Motivated by prior works [16, 20], we set the material parameters $\alpha = -0.5$, $\beta = 1$, and $\gamma = 5\alpha = -2.5$. A search for compatible martensite laminates that can form flat and wedge-like A–M interfaces was performed by scanning over the space of average strain states $(\epsilon_{11}, \epsilon_{22}, \epsilon_{13})$, with $\epsilon_{12} = \epsilon_{23} = 0$ in increments of $\gamma/100$; finer steps were used where needed. This allows a direct comparison with the solutions of Lei *et al* [16] in certain special cases. Note that, with the assumption $\mathrm{tr}(\boldsymbol{\epsilon}_i) = 0$, the third direct strain $\epsilon_{33} = -\epsilon_{11} - \epsilon_{22}$.

3.1. Averagely and exactly compatible martensite laminates

Figure 3 shows the points in the strain space $(\epsilon_{11}, \epsilon_{22}, \epsilon_{13})$ at which exactly compatible martensite laminates can form. The tetrahedral region ABCM in figure 3 contains all feasible combinations of $\epsilon_{11}, \epsilon_{22}, \epsilon_{13}$ under the constraint of

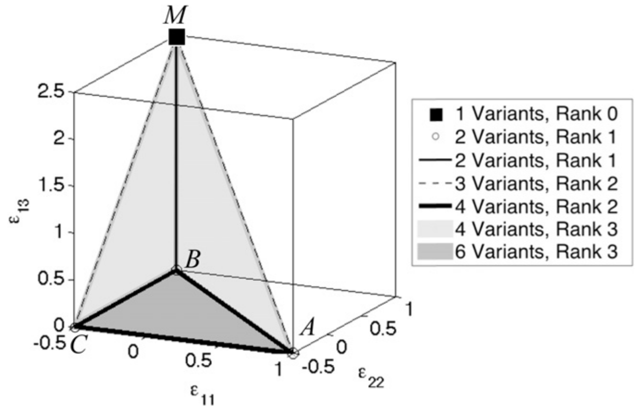

Figure 3. Space of $(\epsilon_{11}, \epsilon_{22}, \epsilon_{13})$ showing states reached by exactly compatible martensite laminates.

equation (5). General points in this region require a rank-5 averagely compatible structure with all six martensite variants present. A schematic structure for a general point in region ABCM is shown in figure 4(a); this adopts the arrangement proposed by DeSimone and James [7], forming a complex pattern of fine twins. However, some special points in this region can form exactly compatible laminates of rank less than 5.

In figure 3, point M represents a single martensite variant, number 4 of equation (6). Points A, B and C require only two variants and allow rank-1 laminates; see figures 4(b) and (c). Points on the lines $\overline{AB}$, $\overline{AC}$ and $\overline{BC}$ need four martensite variants and form rank-2 exactly compatible structures; see figure 4(d). Strain states on line $\overline{BM}$ require only variants 3 and 4 to be present, forming a rank-1 exactly compatible martensite lamination. The lines $\overline{AM}$ (figure 4(e)) and $\overline{CM}$ represent rank-2 exactly compatible laminates with three martensite variants. Finally, typical points in the triangular surfaces ABM, BCM and ABC can be reached with a rank-3 exactly compatible structure. Figure 4(f) and (g) show the structure for a general point in BCM and ABC, respectively.

3.2. Martensite structures that can form a flat A–M interface

The formation of a flat, averagely compatible, A–M interface relies upon the martensite structure having an average strain state $\boldsymbol{\epsilon}$ with a zero middle eigenvalue. In the strain space $(\epsilon_{11}, \epsilon_{22}, \epsilon_{13})$, this condition is satisfied when

$$\epsilon_{22} = 0 \qquad \text{or} \tag{9}$$

$$\epsilon_{11}^2 + \epsilon_{11}\epsilon_{22} + \epsilon_{13}^2 = 0. \tag{10}$$

The strain states within region ABCM of figure 3 that satisfy equations (9) or (10) form the set of points, lines and surfaces shown in figure 5. Rectangle KEHL arises from equation (9), while curved surfaces JDOF and OGI come from solutions to equation (10). All the points on line $\overline{KL}$, inside rectangle KEHL and inside the curved surfaces JDOF, OGI allow only averagely compatible martensite laminates. For example, the martensite laminate shown in figure 4(a) is in the rectangle KEHL; figure 6(a) shows a rank-6 structure containing both

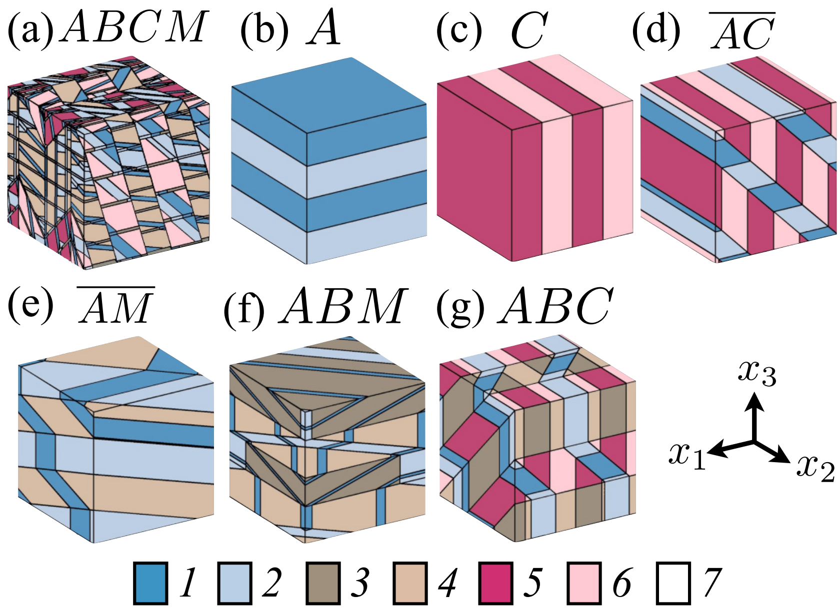

Figure 4. Example microstructures corresponding to (a) points in the region ABCM, (b) point A, (c) point C, (d) line $\overline{\text{AC}}$, (e) line $\overline{\text{AM}}$, (f) surface ABM and (g) surface ABC in figure 3. Different colours/shades indicate phase numbers.

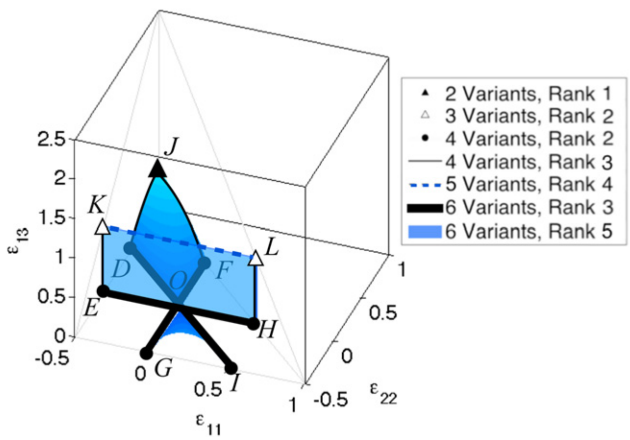

Figure 5. Microstructure map for martensite strain states in the space (ϵ_{11}, ϵ_{22}, ϵ_{13}) that can form flat A–M interfaces.

the rank-5 martensite laminate of figure 4(a) and the austenite phase with strain state at point O ($\boldsymbol{\epsilon} = \mathbf{0}$), separated by a flat A–M interface. In figure 6 the austenite phase is shown translucently to reveal the martensite pattern on the A–M interface. Moving the flat A–M phase boundary scales the average strain state between zero and the strain state of the pure martensite laminate.

Exactly compatible martensite laminates that can form flat A–M interfaces also exist. All the points D . . . L and solid lines shown joining them in figure 5 represent the strain states at which this can happen. Examples taken from lines $\overline{\text{LO}}$, $\overline{\text{FG}}$ and $\overline{\text{JO}}$ and from surface FJO are shown in figures 6(b)–(e). Note that the martensite structures in figures 6(b)–(d) match those of figures 4(e)–(g). It is also interesting to note that some martensite strain states (those on lines $\overline{\text{DI}}$, $\overline{\text{EH}}$ and $\overline{\text{FG}}$) can be achieved in various ways: the strain state does not uniquely determine the pattern of the martensite variants.

The focus is now on point J in figure 5. This is unique in representing the only rank-1 martensite laminate in this strain space that can form a compatible A–M interface. At point J, variants 3 and 4 have the volume fraction ratio 2:3. All strain states on line $\overline{\text{JO}}$ can thus be achieved by the laminate structure shown in figure 6(e), through varying the volume fraction of austenite phase. The corresponding tree diagram is that of figure 1. It is worthwhile to compare the laminate on $\overline{\text{JO}}$ with the structure generated by a two-dimensional phase field calculation, done by Lei *et al* [16]. A zig-zag A–M interface is generated by their model resulting from the energy minimization due to the incompatibility between austenite and martensite phases [16, 22]. However, it is of interest that a similar laminate structure with a flat A–M interface is obtained under the assumption of planar interfaces in the current work.

3.3. Martensite structures that can form wedge-like A–M interfaces

By using the procedure described in sections 2.2 and 2.3, the strain space (ϵ_{11}, ϵ_{22}, ϵ_{13}) was searched for structures which satisfy the conditions for wedge-like A–M interfaces. The results, shown in figure 7, consist of several points and straight lines in the strain space. In most cases, the corresponding martensite structures are averagely compatible with a rank-5 DeSimone–James type arrangement [7]. However, certain special strain states allow for exactly compatible martensite laminates of rank 3 which can form wedge shaped A–M boundaries. Points D . . . I and lines $\overline{\text{KE}}$ and $\overline{\text{LH}}$ require four martensite variants to be present. The conditions for wedge-like A–M interfaces are then satisfied provided that the martensite adopts a DeSimone–James type arrangement. Figure 8(a) shows an example structure corresponding to martensite at point D in the strain space. By moving

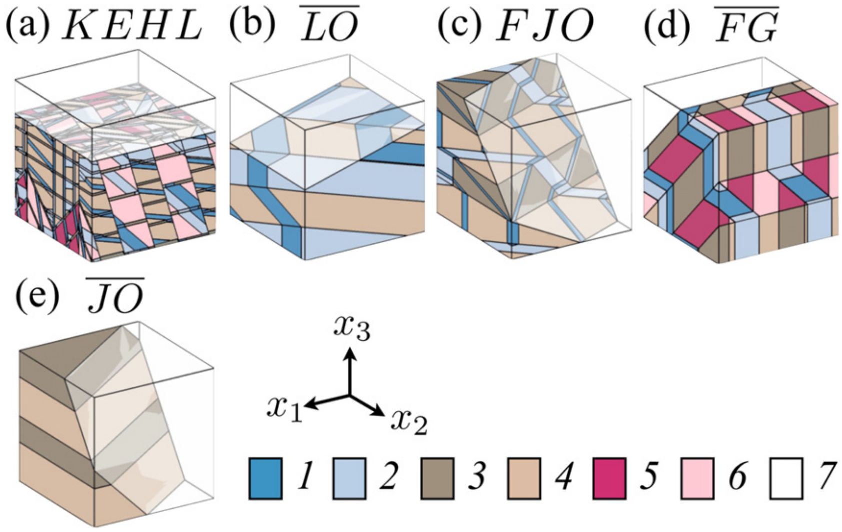

Figure 6. Example microstructures with flat A–M interfaces, corresponding to (a) points in rectangle KEHL, (b) line $\overline{\text{LO}}$, (c) surface FJO, (d) line $\overline{\text{FG}}$ and (e) line $\overline{\text{JO}}$ in figure 5.

the wedge-like A–M interface, the average strain state of the austenite–martensite mixture varies along the line $\overline{\text{DO}}$. Similar structures can also be found for lines $\overline{\text{EO}}$, $\overline{\text{FO}}$, . . . , $\overline{\text{IO}}$. Figure 8(b) shows another example of wedge microstructure, corresponding to surface KOE in figure 7. The martensite again adopts a DeSimone–James arrangement. Interestingly, in these two cases (figures 8(a), (b)) the martensite laminates are exactly compatible. In addition, it is worth noting that the strain states for points D · · · I could form rank-2 exactly compatible martensite laminates, as discussed in section 3.2. However, those laminates consist of substructures that cannot form any flat A–M interface. This violates a requirement for wedge-like A–M interfaces. Points on lines $\overline{\text{DF}}$, $\overline{\text{EG}}$ and $\overline{\text{HI}}$ require six martensite variants. They can adopt rank-3 exactly compatible structures that form wedge-like A–M interfaces. Figure 8(c) shows an example structure with average strain corresponding to a typical point on surface DOF.

All the remaining martensite strain states in $(\epsilon_{11}, \epsilon_{22}, \epsilon_{13})$ space that can form wedge-like A–M interfaces are identified in figure 7 using dashed lines. In each case the martensite structure adopts a high rank, averagely compatible arrangement, resulting in very complicated microstructure patterns. Two examples are shown in figures 8(d) and (e). Finally, returning to the structure that was shown in figure 2, note that this also contains an exactly compatible martensite structure and wedge-like A–M interfaces. However, the strain state corresponding to this martensite structure lies outside the $(\epsilon_{11}, \epsilon_{22}, \epsilon_{13})$ strain space we are currently considering; we have searched only a section of the space of all possible strain states to illustrate the method.

4. Conclusion

In this work, compatibility theory has been used to identify a wide range of martensite laminates that can form in shape memory materials in the cubic–orthorhombic crystal system. The methods employed are powerful in allowing a search

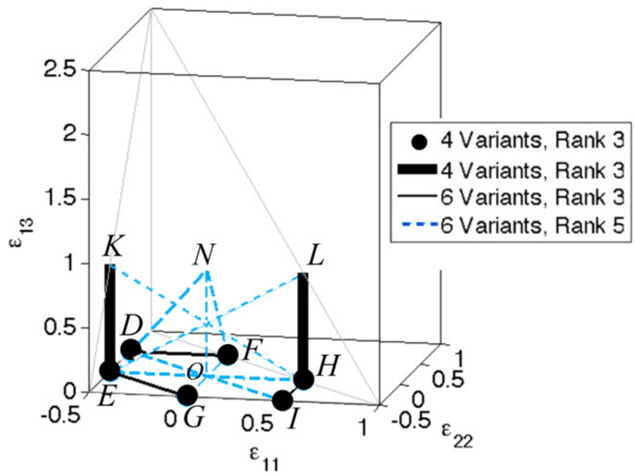

Figure 7. Microstructure map for martensite strain states in the space $(\epsilon_{11}, \epsilon_{22}, \epsilon_{13})$ that can form wedge-like A–M interfaces.

of strain space that rapidly finds both exactly and averagely compatible multi-rank laminate arrangements of martensite and austenite. To illustrate the approach, a search for flat, averagely compatible A–M phase boundaries and wedge-like structures that can form wavy A–M interfaces was carried out. A number of such structures were found, which could be of significance in engineering the microstructure of alloys that can transform smoothly between austenite and martensite. The search method is readily applicable to a range of shape memory alloy crystal systems.

Acknowledgments

This work was supported by the Engineering and Physical Sciences Research Council grant numbers EP/G065233/1 and EP/G004676/1. Shu is glad to acknowledge the support from NTU and from TW NSC (100-2628-E-002-034-MY3). JEH and NTT wish to thank Professors Y C Shu and Jay Shieh

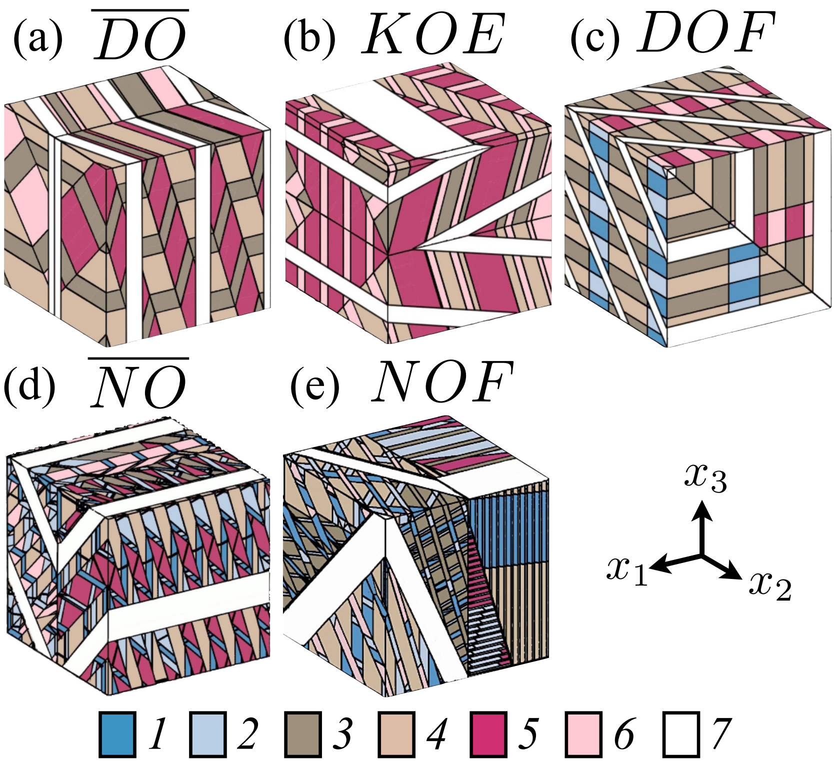

Figure 8. Example microstructures with wedge-like A–M interfaces, corresponding to (a) line $\overline{\mathrm{DO}}$, (b) surface KOE, (c) surface DOF, (d) line $\overline{\mathrm{NO}}$ and (e) surface NOF in figure 7.

for their helpful discussions during their visit to National Taiwan University. NTT also thanks Mr Lei for advice and information.

References

[1] Bhattacharya K 2003 *Microstructure of Martensite: Why it Forms and How it Gives Rise to the Shape-Memory Effect* (Oxford: Oxford University Press)
[2] Dong J W 2004 Shape memory and ferromagnetic shape memory effects in single-crystal Ni_2MnGa thin films *J. Appl. Phys.* **95** 2593
[3] Ball J M and James R D 1987 Fine phase mixtures as minimizers of energy *Arch. Ration. Mech. Anal.* **100** 13–52
[4] Hane K F and Shield T W 1999 Microstructure in the cubic to monoclinic transition in titanium–nickel shape memory alloys *Acta Mater.* **47** 2603–17
[5] Hane K F and Shield T W 2000 Microstructure in a cubic to orthorhombic transition *J. Elast.* **59** 267
[6] Bhattacharya K and James R D 1999 A theory of thin films of martensitic materials with applications to microactuators *J. Mech. Phys. Solids* **47** 531–76
[7] DeSimone A and James R D 2002 A constrained theory of magnetoelasticity *J. Mech. Phys. Solids* **50** 283–320
[8] Chu C and James R D 1995 Analysis of microstructures in Cu–14.0%Al–3.9%Ni by energy minimization *J. Phys. IV* **05** C8-143–9
[9] Abeyaratne R, Chu C and James R D 1996 Kinetics of materials with wiggly energies: theory and application to the evolution of twinning microstructures in a Cu–Al–Ni shape memory alloy *Phil. Mag.* A **73** 457–97
[10] Zhang J X and Chen L Q 2005 Phase-field model for ferromagnetic shape-memory alloys *Phil. Mag. Lett.* **85** 533–41
[11] Levitas V I, Idesman A V and Preston D L 2004 Microscale simulation of martensitic microstructure evolution *Phys. Rev. Lett.* **93** 105701
[12] Shu Y C and Yen J H 2007 Pattern formation in martensitic thin films *Appl. Phys. Lett.* **91** 021908
[13] Shu Y C and Yen J H 2008 Multivariant model of martensitic microstructure in thin films *Acta Mater.* **56** 3969–81
[14] Li L J, Li J Y, Shu Y C, Chen H Z and Yen J H 2008 Magnetoelastic domains and magnetic field-induced strains in ferromagnetic shape memory alloys by phase-field simulation *Appl. Phys. Lett.* **92** 172504
[15] Li L J, Lei C H, Shu Y C and Li J Y 2011 Phase-field simulation of magnetoelastic couplings in ferromagnetic shape memory alloys *Acta Mater.* **59** 2648–55
[16] Lei C H, Li L J, Shu Y C and Li J Y 2010 Austenite–martensite interface in shape memory alloys *Appl. Phys. Lett.* **96** 141910
[17] Roytburd A L, Kim T S, Su Q M, Slutsker J and Wuttig M 1998 Martensitic transformation in constrained films *Acta Mater.* **46** 5095–107
[18] Goldsztein G H 2001 The effective energy and laminated microstructures in martensitic phase transformations *J. Mech. Phys. Solids* **49** 899–925
[19] Tsou N T and Huber J E 2010 Compatible domain structures and the poling of single crystal ferroelectrics *Mech. Mater.* **42** 740–53
[20] Tsou N T, Huber J E and Shu Y C 2011 A model of compatible twin patterns in shape memory alloys *SMASIS2011: ASME 2011 Conf. on Smart Materials, Adaptive Structures and Intelligent Systems* vol 1 SMASIS2011–4954
[21] Tsou N T and Huber J E 2010 Compatible domain arrangements and poling ability in oriented ferroelectric films *Continuum Mech. Thermodynam.* **22** 203–19
[22] Stupkiewicz S, Maciejewski G and Petryk H 2007 Low-energy morphology of the interface layer between austenite and twinned martensite *Acta Mater.* **55** 6292